Journal of Magnetic Resonance 262 (2016) 15–19

Contents lists available at ScienceDirect

Journal of Magnetic Resonance

journal homepage: www.elsevier.com/locate/jmr

High-frequency pulsed ENDOR spectroscopy of the NV^- centre in the commercial HPHT diamond

B.V. Yavkin *, G.V. Mamin, S.B. Orlinskii

Kazan Federal University, Institute of Physics, 420008 Kazan, 18 Kremlyovskaya St, Russian Federation

ARTICLE INFO

Article history:
Received 17 August 2015
Revised 9 November 2015
Available online 2 December 2015

Keywords:
W-band
ENDOR
Diamond
Nitrogen-vacancy centre
Hyperfine interaction
Quadrupole interaction

ABSTRACT

This work reports direct 94 GHz ENDOR spectroscopy of the ^{14}N nuclei in the NV^- centre in single-crystal diamond. Roadmaps of ENDOR frequencies were measured and hyperfine/quadrupole interaction parameters were obtained, with $A_{X,Y} = -2.7$ MHz, $A_Z = -2.2$ MHz and $P = -4.8$ MHz. The sign and value of each parameter was calculated using spin Hamiltonian matrix diagonalization, first and second order perturbation theory and confirmed experimentally. Magnetic field magnitude was measured by ^{13}C ENDOR signal with 0.02% precision or 0.5 mT. The orientation of quadrupole, hyperfine and fine structure tensors are the same within error of experiment, *g*-factor is isotropic.

1. Introduction

The study of NV^- centres has a long story from 1960-ies, firstly started from the optical characterisation [1] and then proceeds by EPR spectroscopy. Comparative analysis of the optical transitions and EPR lines was provided as early as 1970 in the work of Wyk [2], but correct interpretation of observed light-induced behaviour was done by [3], and relevant energy level scheme was proposed. The next major insight into the study of NV enters was made in the pioneering work [4] of the single-spin spectroscopy via NV centres. From that time, in the middle of 90-s, the NV centres was tried in many applications e.g. towards nanoscale system [5] as a highly efficient probe or qubit system [6]. Nowadays single nuclear spin spectroscopy was demonstrated even at room temperature [7,8] by means of coupling nuclear spin to the NV^- electronic spin, which is used to read-out nuclear spin state. The same recipe is used to prepare quantum qubit state using NV^- centre in diamond [9]. Therefore, to be reliable probe (or a qubit component) NV^- centre magnetic parameters, especially hyperfine and quadrupole tensors, have to be determined precisely. There are well-spread values of these spectroscopic parameters that are used routinely [10] in literature, but we haven't found a single work that determines *A* and *P* (hyperfine and quadrupole, correspondingly) on the solid basis of angle-dependent ENDOR spectroscopy. Moreover, there is a disagreement on the value and especially sign of *A* and *P* parameters. Thus, authors decided to fill this gap and provide results of their spectroscopic investigation of NV^- centre in particular commercial diamond by high-frequency ENDOR.

2. Materials and methods

Sample for the study was as used in work [11]. A micron-sized (of about 250 μm) diamond single crystal was fabricated commercially by Element Six using HPHT (high pressure high temperature) synthesis. The initial concentration of the nitrogen impurities in the sample was estimated to be of $\approx 5 * 10^{18}$ cm^{-3}. The crystal was subjected to electron irradiation (≈2 MeV) with the flux density of $\approx 10^{18}$ cm^{-2} followed by annealing in the hydrogen atmosphere at $T = 800$ °C for 2 h.

The experimental work of the paper was done on the Bruker Elexsys E680 machine operating at 94 GHz in the pulsed regime. Pulsed ENDOR, recorded by Mims pulse sequence is easier to implement and detect compared to the CW ENDOR (although there is a beautiful CW ENDOR study of P1 centre in diamond [12]), because the relaxation times (that usually have to be balanced with each other and temperature of the experiment) are directly involved to the Mims pulse sequence; in addition, high-frequency ENDOR spectrum has large frequency span and is easier to interpret. Field-swept EPR spectra were acquired using two-pulse Hahn echo sequence $\pi/2$–τ–π with $\pi/2$ pulse of 48 ns and $\tau = 280$ ns. ENDOR spectra were measured by Mims pulse sequence $\pi/2$–τ–$\pi/2$–T–$\pi/2$ with $\pi/2$ pulse of 48 ns (if other value is not mentioned) and $\tau = 280$ ns and RF pulse of 150 μs inserted in the time interval T

* Corresponding author.
E-mail address: boris.yavkin@gmail.com (B.V. Yavkin).

http://dx.doi.org/10.1016/j.jmr.2015.11.005
1090-7807/

between second and third microwave pulses. Angular-dependent measurements were done using uniaxial goniometer with step precision of 0.3 degrees.

Experiments were carried out at 300 K in the dark or under continuous illumination with 640 nm laser of 40 mW emitting power. Light was reaching the sample trough the fibre, incident laser power on the sample surface was estimated to about 400 μW (although reflections from the inner microwave cavity surfaces and tube walls are not taken into account). There was no detectable difference in the EPR or ENDOR line position or shape between the dark and illuminated type of experiment (see Fig. SI4 in supporting material for details). Therefore, most of the experiments were done under continuous illumination.

Modelling of the EPR and ENDOR line position was carried out with EasySpin package for Matlab [13].

3. Results and discussion

First of all, let us discuss illumination of the sample with laser light. An unusual choice of laser wavelength of 640 nm instead of a commonly used 532 nm is explained, most probably, by the ZPL (zero-phonon line) shift towards 640 nm at room and above temperatures. That was recently shown by PL (photoluminescence) measurements [14]. The use of laser illumination is to create a spin-polarised ground state and enhance EPR and ENDOR signals. In our case, the light-induced EPR spectra under 640 nm were six times larger in magnitude compared to the dark experiment (in the $B||\langle 1\,1\,1\rangle$ orientation) and two times compared to 532 nm illumination. Since illumination of the sample with certain wavelength leads to enhanced EPR signal intensity, almost all measurements were conducted under the illumination with continuous laser light. However in order to check whether the lineshape or position (both EPR and ENDOR) is not affected by the light, some control experiments were carried out in the dark. There were no detectable changes in line position and shape, as mentioned above, and one could observe confirmation on Fig. SI4.

Spin Hamiltonian of NV^- system is axially-symmetric, electronic spin $S = 1$, and nuclear spin I of ^{14}N is also 1. In the assumption of anisotropic hyperfine interaction parameter A and axial quadrupole interaction P spin Hamiltonian is presented in Eq. (1)

$$H = g\beta \mathbf{BS} + D\left[S_Z^2 - \frac{1}{3}S(S+1)\right] - g_N\beta_N \mathbf{BI} + A_{\parallel}S_Z I_Z + A_{\perp}(S_X I_X + S_Y I_Y) + P\left[I_Z^2 - \frac{1}{3}I(I+1)\right]. \quad (1)$$

Angular dependence of EPR and ENDOR line position are presented in Fig. 1a and b correspondingly. We did not present a full angular variation of NV defect EPR lines (could be found elsewhere, e.g. in [15] or in supporting information to this article, see Fig. SI1) but only of the pair of lines that approach $\langle 1\,1\,1\rangle$ axis closer than others, i.e. only one of the four possible crystallographic orientation of NV defect in diamond. The degree of closeness is estimated from the line splitting which at extreme was calculated to be 200.5 mT, i.e. within a few degrees from the true $B||\langle 1\,1\,1\rangle$ orientation. The difference between measured splitting and splitting determined by actual D parameter (approx. 205.5 mT) leads to 7.3(3) degree of misalignment, which introduce the 0.1 MHz error to the hyperfine and quadrupole parameters. The absolute field measurements precision was 0.5 mT, as will be stated further in the text. We therefore will not return to the discussion of the correct orientation of the sample and accept the condition we achieved as $B||\langle 1\,1\,1\rangle$, because the more precise placement of such a small sample within the W-band tube seems to be impractical in current work. In addition, recent publication on the high-frequency ODMR study of NV centres in diamond reported the same degree of magnetic field alignment precision [16].

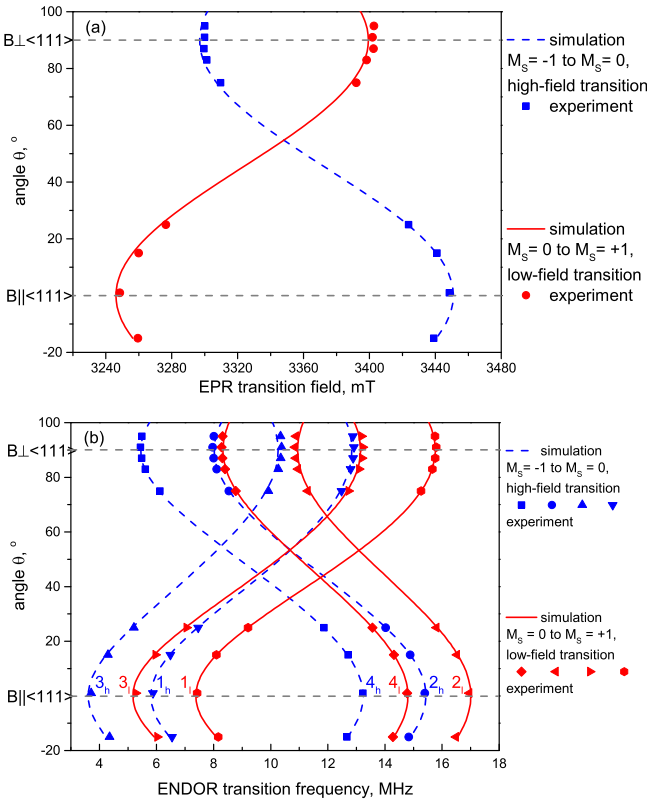

Fig. 1. (a) EPR roadmap of two NV^- transitions and (b) corresponding ENDOR frequencies. Solid and dashed lines on both figures represent simulated roadmap, scattered points represent experimental roadmap. The additional numbers from $1_{h,\,l}$ to $4_{h,\,l}$ denote ENDOR frequencies that were measured near to $B||\langle 1\,1\,1\rangle$ orientation. These ENDOR frequencies will be considered further during the hyperfine parameters sign determination (Fig. 2) and energy level scheme discussion (Fig. 3). Note that EPR transitions presented here correspond to only one of the four possible crystallographic types of NV centre.

In order to extract spin-Hamiltonian parameters of hyperfine interaction, the mathematical modelling of the experimental EPR transition fields and ENDOR transition frequencies using full matrix diagonalization of spin Hamiltonian from Eq. (1) was carried out. From the modelling procedure we determined that $g_{iso} = 2.0028(1)$, $D = 2.87(1)$ GHz, $A_{X,Y} = -2.7(1)$ MHz, $A_Z = -2.2(1)$ MHz and $P = -4.8(1)$ MHz. The quadrupole parameter P equals to $3/2P_Z$ and quadrupole interaction tensor component are $P_X = P_Y = 1.6$ MHz, $P_Z = -3.2$ MHz, and $e^2Qq/h = -6.4$ MHz. D, A and P tensors were considered to be collinear.

The D value and sign are well known and are in agreement with data from known literature but the hyperfine and especially quadrupole magnitude and sign diverge significantly from the reported previously (see Table 1). Let us see how these parameters were determined and confirmed experimentally. The purpose of group

Table 1
Hyperfine A and quadruple P interaction parameters.

Reference	$A_{X,Y}$ (MHz)	A_Z (MHz)	P (MHz)
This work	−2.7 ± 0.1	−2.2 ± 0.1	−4.8 ± 0.1
Loubser and Wyk [2]	–	+2.32 ± 0.01	–
Manson et al. [17]	−2.3	−2.3 ± 0.1	−5.1 ± 0.1
He et al. [18]	+2.30 ± 0.02	+2.10 ± 0.02	−5.04 ± 0.05
Smeltzer et al. [19]	−2.162 ± 0.002	−2.162 ± 0.002	−4.945 ± 0.005
Felton et al. [20]	−2.70 ± 0.07	−2.14 ± 0.07	−5.01 ± 0.06
Steiner et al. [21]	−2.3	−2.3	5.1 ± 0.1
Shin et al. [22]	+2.1	+2.3	−5.04
Chen et al. [23]	−2.162 ± 0.002	−2.62 ± 0.05	−4.945 ± 0.005

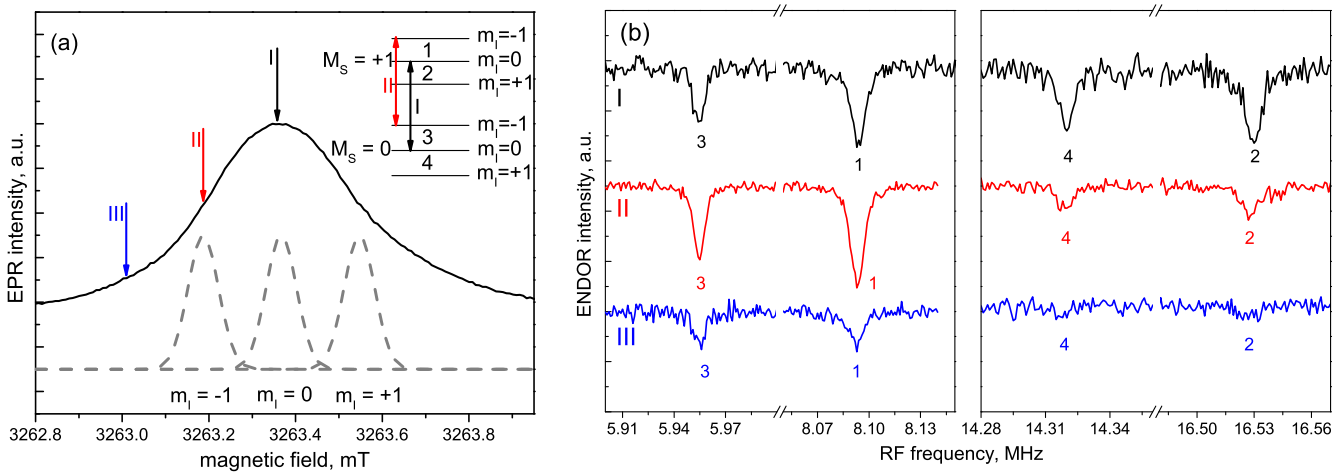

Fig. 2. (a) Single EPR line of the NV centre in B||⟨1 1 1⟩ orientation and (b) corresponding ENDOR spectra. Arrows and numbers on the (a) denote field position at which ENDOR spectra (b) were measured.

of Eq. (2) and Fig. 2 is to illustrate how the sign determination was done in this work experimentally. This set of equations represents a little bit simplified but transparent approximation on the ENDOR frequencies will tell us the sign of hyperfine interaction of unpaired electron and ^{14}N nuclei of the NV$^-$ system. The second-order corrections due to axial hyperfine interaction A are less than 0.1 kHz and considered irrelevant. Please note that Eqs. (2a) and (2b) are written for $B||\langle 1\,1\,1\rangle$ only. Therefore, first-order approximation there are eight distinct ENDOR frequencies listed below (Eq. 2a and 2b hereafter):

In the $Ms = 0$ to $Ms = 1$ EPR transition (low field transition, because D is positive):

$$f_1 = \frac{1}{h}[E(1,-1) - E(1,0)] = f_{larmor}^{lowfield} - A + P, \tag{2a}$$
$$f_2 = \frac{1}{h}[E(1,0) - E(1,1)] = f_{larmor}^{lowfield} - A - P,$$
$$f_3 = \frac{1}{h}[E(0,-1) - E(0,0)] = f_{larmor}^{lowfield} + P,$$
$$f_4 = \frac{1}{h}[E(0,0) - E(0,1)] = f_{larmor}^{lowfield} - P.$$

In the $Ms = -1$ to $Ms = 0$ EPR transition (high field transition):

$$f_5 = \frac{1}{h}[E(0,-1) - E(0,0)] = f_{larmor}^{highfield} + P,$$
$$f_6 = \frac{1}{h}[E(0,0) - E(0,1)] = f_{larmor}^{highfield} - P,$$
$$f_7 = \frac{1}{h}[E(-1,-1) - E(-1,0)] = f_{larmor}^{highfield} + A + P,$$
$$f_8 = \frac{1}{h}[E(-1,0) - E(-1,1)] = f_{larmor}^{highfield} + A - P. \tag{2b}$$

Therefore, if A is positive, the highest ENDOR frequency will be observed on the high-field EPR transition, irrelevant on the sign of quadrupole interaction P. Otherwise, the highest ENDOR frequency would be observed on the low-field EPR transition. In experiment, e.g. Fig. 1b, the low-field EPR transition corresponds to the highest ENDOR frequency, which defines A sign as negative.

It is clear that previous simplified consideration could allow us only to determine the sign of hyperfine constant A, but quadrupole interaction parameter P remains unknown. In order to determine the sign of quadrupole interaction, the $Ms = 0$ to +1, i.e. low-field EPR transition ($B||\langle 1\,1\,1\rangle$) will be considered in more detail and ENDOR transitions magnitude will be discussed in depth. The sign of hyperfine parameter A is negative, as we have determined above, therefore the energy levels splitted by the nuclear magnetic moment will be sequenced as $m_I = -1$, 0, 1 from lower magnetic field to higher, respectively. The measured EPR line and respective ENDOR frequencies are presented in Fig. 2 below. To increase the spectral selectivity microwave pulse length was increased to $\pi/2 = 120$ ns, which roughly corresponds to 0.28 mT of the EPR linewidth that contributes to the ENDOR spectrum.

According to level scheme shown on inset of Fig. 2a we first excite central ($m_I = 0$) transition where all ENDOR frequencies contribute equally. Then magnetic field was shifted to the $m_I = -1$ position and ENDOR once again was recorded. The significant contribution of the high-frequency (ca. 14.32 MHz and 16.53 MHz) ENDOR lines rises from the partial excitation of $m_I = 0$ transition (because of the finite spectral width of the pulse 0.28 mT as was mentioned before). Moving even further away from the central transition suppress high-frequency part almost completely, thereby confirming the chosen energy scheme and P sign as negative.

In addition, one could refer to Fig. SI5 and additional explanation in the supporting material.

Having determined values and signs of all relevant spin Hamiltonian parameters, one could plot the energy level scheme of NV$^-$ defect with accent on the hyperfine and quadrupole interaction of ^{14}N nucleus. Note that the energy level scheme and experimental ENDOR frequencies are plotted only for one orientation $B||\langle 1\,1\,1\rangle$ due to complexity of arbitrary orientation scheme and corresponding ENDOR lines.

The combined report on the hyperfine interaction parameter is present in Table 1 along with most citing works on the same subject published before. The data and references in Table 1 partly reproduce the work of Doherty et al. [10], only expanded by some recent references. The idea to present so many reference works was to show ever present ambiguity on the corresponding subject of hyperfine and quadrupole parameters.

Let us discuss how the values of P and A obtained in current article are related to the reference works.

According to the set of Eq. (2), the quadrupole and hyperfine interaction parameters could be determined if larmor frequency is known. For instance, one could consider the low-field EPR line and corresponding four ENDOR frequencies in the nearest to $B||\langle 1\,1\,1\rangle$ orientation (denoted by numbers from 1 to 4 and letter l in the Fig. 1a and b). The ENDOR frequencies of ^{14}N and ^{13}C are presented in Fig. 4 below, ENDOR spectra recorded at the low field EPR component in the magnetic field of 3246.2 mT.

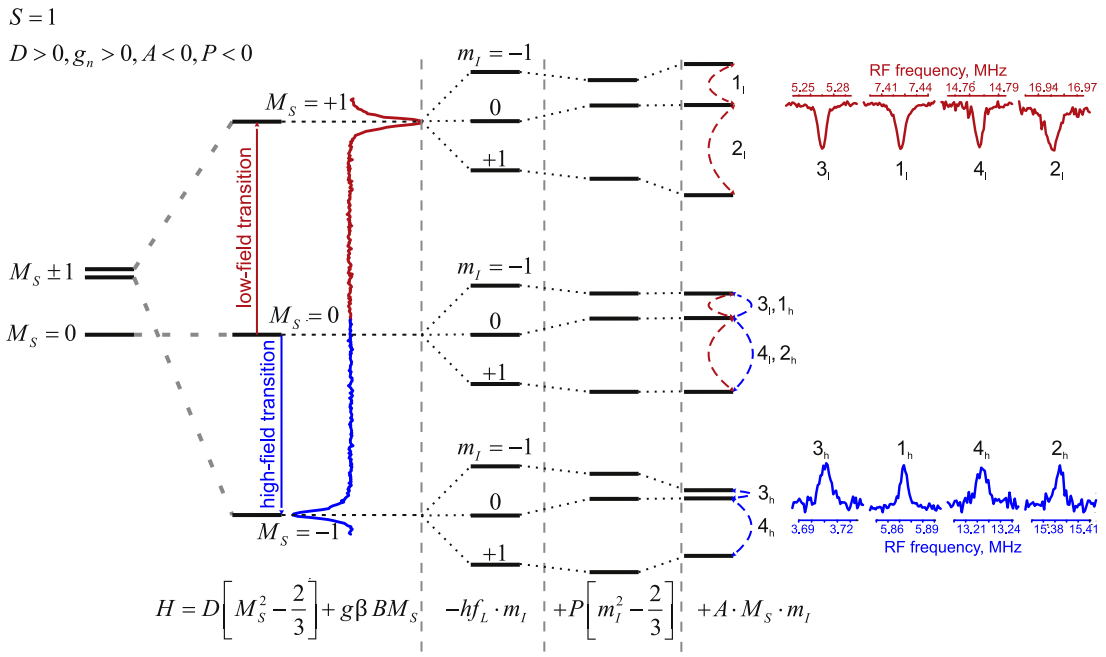

Fig. 3. Energy levels of the NV^- with hyperfine structure of the nitrogen nuclei. The inset in the right part of the figure shows experimental ENDOR frequencies at the B||⟨1 1 1⟩ orientation.

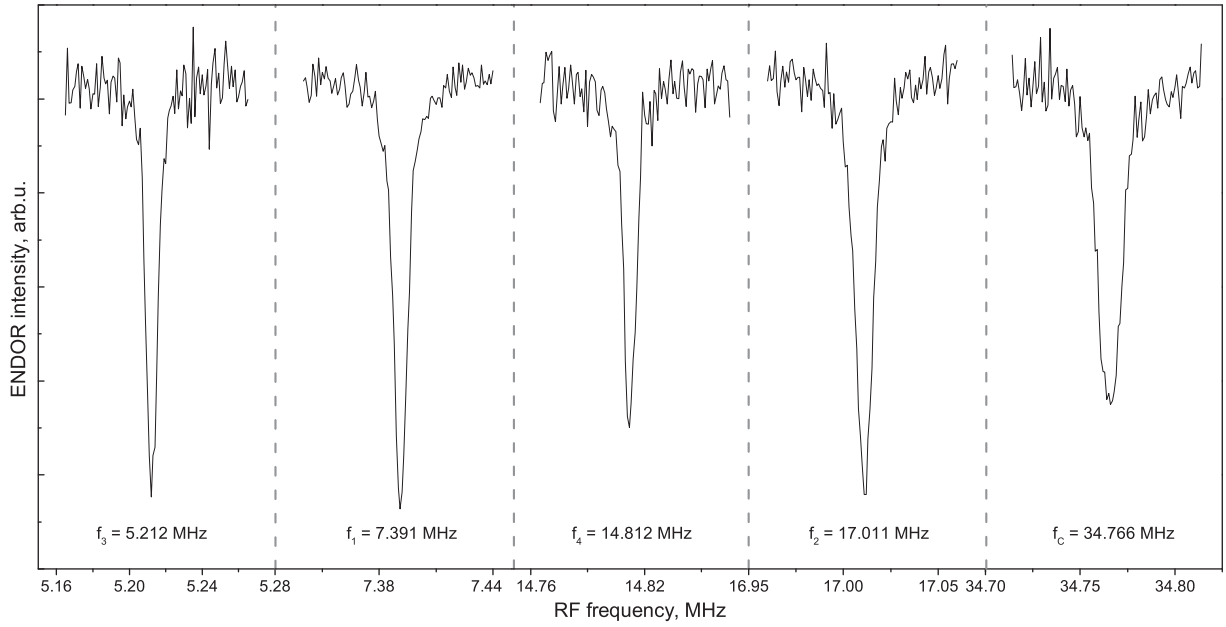

Fig. 4. ENDOR spectra of ^{14}N and ^{13}C nuclei taken at low-field EPR transition in magnetic field 3246.2 mT.

According to the set of Eq. (2), $f_l = (f_3 + f_4)/2$, thus f_l = 10.012 - MHz, which corresponds to the magnetic field $B_0(^{14}N)$ = 3253.1 mT (which is 7 mT offset from the real magnetic field). At the same time, the ^{13}C ENDOR frequency that has no hyperfine interaction in the vicinity of larmor frequency may be used as a reliable marker of the magnetic field magnitude. According to ^{13}C ENDOR signal, magnetic field is equal to $B_0(^{13}C)$ = 3246.6 mT, within 0.5 mT from the experimental value stated above. Therefore, larmor frequency of ^{14}N could not be determined correctly solely from ^{14}N ENDOR spectrum and additional frequency reference is important. For example, slight misalignment (i.e. reported 8 degrees of deviation from true B||⟨1 1 1⟩ orientation) could be the reason for incorrect larmor frequency reading. The ^{13}C ENDOR of distant carbon nuclei, as stated above could be reliable independent measurement, because its signal located at larmor frequency and is structureless, therefore it is not affected by any angular-dependent spin Hamiltonian parameters (like anisotropic hyperfine interaction) and represents only actual magnitude of external magnetic field applied to the sample.

According to set of Eqs. (2a) and (2b) hyperfine and quadrupole parameters can be calculated without calculation of larmor frequency, i.e. the quadrupole parameter P determined by Eq. (2) will be $P = (f_3 - f_4)/2 = -4.8$ MHz and hyperfine parameter $A_{||} = (f_4 - f_2)$ or $(f_3 - f_1) = -2.18$–2.2 MHz. It is seen that both hyperfine

parameter A and quadrupole P are in agreement with references of Table 1.

Now we would like to address in more details how A and P parameters were estimated previously and why current research could be considered as important additional contribution. First, the closeness of hyperfine, quadrupole and larmor frequencies in low magnetic field experiments [17–19,21,22] makes attribution of the observed ENDOR frequencies to correct m_I sublevels somewhat tricky and troublesome (ENDOR frequencies are not centred on the larmor frequency); this is important in the question of absolute signs of A and P parameters, that were determined in current study unambiguously relative to the D sign. Second, the elegant way of using forbidden EPR transitions to estimate hyperfine and quadrupole interaction that was demonstrated by Felton et al. [20] and Chen et al. [23] is hard to implement at higher microwave frequency and analysis of the forbidden EPR transition spectrum is much harder in comparison with high-frequency ENDOR that shown to be almost straightforward.

4. Conclusion

In conclusion, the high-frequency ENDOR measurements of the hyperfine structure of the nitrogen nuclei of the NV^- centre was done and spin Hamiltonian parameters that contributes to the hyperfine interaction, A and P tensors, was determined. The magnetic field was determined with precision up to 0.02% (or 0.5 mT) using ENDOR transition of ^{13}C as marker. Results of the current work are considered to be in agreement with majority of works on the hyperfine value of $A_{X,Y} = -2.7$ MHz and $A_Z = -2.2$ MHz and quadrupole parameter $P = -4.8$ MHz. The signs of A and P parameters were determined experimentally relative to the sign of zero-field splitting D.

Acknowledgments

Authors would like to acknowledge V. Soltamov and P. Baranov for providing the diamond crystal and stimulating discussions during the article preparation. Authors are grateful to Alexej Orlinskii for his help in manuscript preparation. The financial support of the RFBR project number 14-02-31881 mol_a is appreciated. In addition, this work was partially funded by the subsidy allocated to Kazan Federal University for the project part of the state assignment in the sphere of scientific activities.

Appendix A. Supplementary material

Supplementary data associated with this article can be found, in the online version, at http://dx.doi.org/10.1016/j.jmr.2015.11.005.

References

[1] G. Davies, M.F. Hamer, Optical studies of the 1.945 eV vibronic band in diamond, Proc. R. Soc. Lond. A 348 (1976) 285–298.
[2] J.H.N. Loubser, J.A.V. Wyk, Electron spin resonance in the study of diamond, Reports Prog. Phys. 41 (8) (1978) 1201.
[3] D.A. Redman, S. Brown, R.H. Sands, S.C. Rand, Spin dynamics and electronic states of NV-centers in diamond by EPR and four-wave-mixing spectroscopy, Phys. Rev. Lett. 67 (24) (1991) 3420–3423.
[4] A. Gruber, A. Dräbenstedt, C. Tietz, L. Fleury, J. Wrachtrup, C. von Borczyskowski, Scanning confocal optical microscopy and magnetic resonance on single defect centers, Science 276 (1997) 2012–2013.
[5] Viva R. Horowitz, B.J. Alemán, D.J. Christle, A.N. Cleland, D.D. Awschalom, Electron spin resonance of nitrogen-vacancy centers in optically trapped nanodiamonds, PNAS 109 (34) (2012) 13493–13497.
[6] J. Wrachtrup, S. Ya Kilin, A.P. Nizovtsev, Quantum computation using the ^{13}C nuclear spins near the single NV defect center in diamond, Opt. Spectrosc. 3 (2001) 429–437.
[7] H.J. Mamin, M. Kim, M.H. Sherwood, C.T. Rettner, K. Ohno, D.D. Awschalom, D. Rugar, Nanoscale nuclear magnetic resonance with a nitrogen-vacancy spin sensor, Science 339 (2013) 557–560.
[8] T. Staudacher, F. Shi, S. Pezzagna, J. Meijer, J. Du, C.A. Meriles, F. Reinhard, J. Wrachtrup, Nuclear magnetic resonance spectroscopy on a (5-Nanometer)^3 sample volume, Science 339 (2013) 561–563.
[9] H. Bernien, B. Hensen, W. Pfaff, G. Koolstra, M.S. Blok, L. Robledo, T.H. Taminiau, M. Markham, D.J. Twitchen, L. Childress, R. Hanson, Heralded entanglement between solid-state qubits separated by three meters, Nature 497 (2013) 86–90.
[10] M. Doherty, N.B. Manson, P. Delaney, F. Jelezko, J. Wrachtrup, L.C.L. Hollenberg, The nitrogen-vacancy colour centre in diamond. Available from: <arXiv:1302.3288>.
[11] B.V. Yavkin, G.V. Mamin, S.B. Orlinskii, S.V. Kidalov, F.M. Shakhov, A.Ya. Vul', A. A. Soltamova, V.A. Soltamov, P.G. Baranov, Room-temperature high-field spin dynamics of NV defects in sintered diamonds, Appl. Magn. Reson. 44 (10) (2013) 1235–1244.
[12] A. Cox, M.E. Newton, J.M. Baker, ^{13}C, ^{14}N and ^{15}N ENDOR measurements on the single substitutional nitrogen centre (P1) in diamond, J. Phys.: Condens. Matter. 6 (1994) 551–563.
[13] S. Stoll, A. Schweiger, EasySpin, a comprehensive software package for spectral simulation and analysis in EPR, J. Magn. Reson. 178 (1) (2006) 42–55.
[14] X.-D. Chen, C.-H. Dong, F.-W. Sun, C.-L. Zou, J.-M. Cui, Z.-F. Han, G.-C. Guo, Temperature dependent energy level shifts of nitrogen-vacancy centers in diamond, Appl. Phys. Lett. 99 (16) (2011) 161903.
[15] P.G. Baranov, A.A. Soltamova, D.O. Tolmachev, N.G. Romanov, R.A. Babunts, F. M. Shakhov, S.V. Kidalov, A.Y. Vul', G.V. Mamin, S.B. Orlinskii, N.I. Silkin, Enormously high concentrations of fluorescent nitrogen-vacancy centers fabricated by sintering of detonation nanodiamonds, Small 7 (11) (2011) 1533–1537.
[16] V. Stepanov, F.H. Cho, A. Chathuranga, S. Takahashi, High-frequency and high-field optically detected magnetic resonance of nitrogen-vacancy centers in diamond, Appl. Phys. Lett. 106 (2015) 063111.
[17] N.B. Manson, X.-F. He, P.T.H. Fisk, Raman heterodyne detected electron-nuclear-double-resonance measurements of the nitrogen-vacancy center in diamond, Opt. Lett. 15 (19) (1990) 1094–1096.
[18] X.-F. He, N.B. Manson, P.T.H. Fisk, Paramagnetic resonance of photoexcited NV-defects in diamond. II. Hyperfine interaction with the ^{14}N nucleus, Phys. Rev. B 47 (14) (1993) 8816–8822.
[19] B. Smeltzer, J. McIntyre, L. Childress, Robust control of individual nuclear spins in diamond, Phys. Rev. A 80 (5) (2009) 050302.
[20] S. Felton, A.M. Edmonds, M.E. Newton, P.M. Martineau, D. Fisher, D.J. Twitchen, J.M. Baker, Hyperfine interaction in the ground state of the negatively charged nitrogen vacancy center in diamond, Phys. Rev. B 79 (7) (2009) 075203.
[21] M. Steiner, P. Neumann, J. Beck, F. Jelezko, J. Wrachtrup, Universal enhancement of the optical readout fidelity of single electron spins at nitrogen-vacancy centers in diamond, Phys. Rev. B 81 (3) (2010) 035205.
[22] C.S. Shin, M.C. Butler, H.-J. Wang, C.E. Avalos, S.J. Seltzer, R.-B. Liu, A. Pines, V.S. Bajaj, Optically detected nuclear quadrupolar interaction of ^{14}N in nitrogen-vacancy centers in diamond, Phys. Rev. B 89 (20) (2014) 205202.
[23] Mo. Chen, M. Hirose, P. Cappellaro, Measurement of transverse hyperfine interaction by forbidden transitions, Phys. Rev. B 92 (2015) 020101(R).